THE JOURNAL OF PHYSICAL CHEMISTRY Letters

Cite This: J. Phys. Chem. Lett. 2018, 9, 3416−3424

Letter

pubs.acs.org/JPCL

Tuning the Optoelectronic Properties of Two-Dimensional Hybrid Perovskite Semiconductors with Alkyl Chain Spacers

Claudio Quarti,* Nadège Marchal, and David Beljonne

Laboratory for Chemistry of Novel Materials, University of Mons, Place du Parc, 20, B-7000 Mons, Belgium

Supporting Information

ABSTRACT: Layered two-dimensional organo-metal halide perovskites are currently in the limelight, largely because their versatile chemical composition offers the promise of tunable photophysical properties. We report here on (time-dependent) density functional theory [(TD)DFT] calculations of alkyl-ammonium lead iodide perovskites, where significant changes in the electronic structure and optical properties are predicted when using long versus short alkyl chain spacers. The mismatch between the structural organization in the inorganic and organic layers is epitomized for dodecyl chains that adopt a supramolecular packing similar to that of polyethylene, at the cost of distorting the inorganic frame and, in turn, opening the electronic band gap. These results rationalize recent experimental data and demonstrate that the optoelectronic properties of layered halide perovskite semiconductors can be modified through the use of electronically inert organic saturated chains.

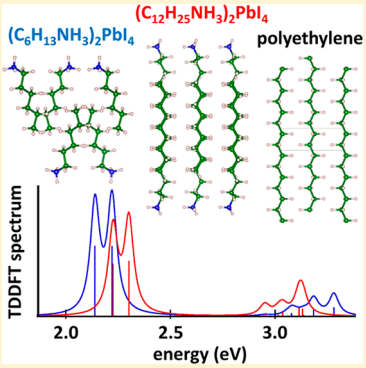

Hybrid organic−inorganic perovskites are currently attracting enormous interest, thanks to their successful use as active layer in photovoltaic applications.[1−8] These materials are characterized by the chemical formula ABX_3 (B = metal cation and X = halide), and their crystalline structure consists of a continuous network of corner-sharing BX_6 octahedra, which is the origin of their unique electronic properties.[9,10] The A cation, instead, guarantees the charge neutrality and occupies the cavity between the PbX_6 octahedra. For this reason, A must satisfy strict geometric rules, mathematically expressed by the Goldschmidt factor tolerance,[11] a fact that strongly reduces its possible choice, originally limited to few small organic compounds (CH_3NH_3, $CH(NH_2)_2$)[12] but recently extended also to some inorganic elements (Cs, Rb) and mixed compounds.[13,14] On the other hand, the relaxation of such a constraint on the size of A and the use of long organic chains results in the breakup of the three-dimensional (3D) perovskite structure and favors the formation of layered compounds, where the perovskite structure is confined in isolated sheets alternated with organic spacers.[15,16] These layered perovskites are currently the focus of intense research activity, largely because the spatial and dielectric confinement of the electrons within single perovskite sheets provides these 2D materials with unique photophysical response. This, together with the much wider chemical flexibility of these compounds compared to their 3D analogues, makes layered organometal perovskite materials attractive for many optoelectronic applications. The excitonic character of these materials, associated with the above-mentioned electronic confinement, results in narrow, effective, and wavelength-tunable photoluminescence, ideal for light-emitting diode (LED) applications.[17−20] Moreover, many layered 2D perovskite are characterized by unresolved broad band light emission, which makes them suitable for white lighting applications.[21−25] Finally, layered 2D perovskites have been successfully used for solar cell applications,[26] with both materials and devices showing improved stability to environmental degradation, compared to their 3D counterparts, but still retaining considerable photovoltaic efficiencies (∼15%).[27,28]

Layered 2D perovskite materials hence embody great potential for technological exploitation. Nevertheless, the understanding of how the optoelectronic response of these materials depends on their detailed crystalline structure and on the choice of their constituents, namely the nature of the A cation, is still at its early stage.[29,30] With the aim of contributing design rules for the detailed control of the optoelectronic response of layered 2D perovskites, we present here the results of electronic structure simulations performed on the hexylammonium lead iodide perovskite $(C_6H_{13}NH_3)_2PbI_4$ and dodecylammonium lead iodide perovskite $(C_{12}H_{25}NH_3)_2PbI_4$. For simplicity, we refer to these compounds as C6PbI and C12PbI, respectively, and to the corresponding organic cation as C6 and C12. These layered perovskite materials have been widely investigated in the past, and their structural[31−33] and optical properties[34−36] are well-documented. Previous DSC and XRD measurements on C6 and C12 single crystals showed that both these materials undergo several transitions in their crystalline arrangement.[31−33] Hence, polymorphism represents a further source of complication in the study of the optoelectronic response of these compounds. In particular, C6 shows a transition from a monoclinic to an orthorhombic phase,[31] by heating above 268 K, while C12 shows the opposite

Received: April 25, 2018
Accepted: June 5, 2018
Published: June 5, 2018

DOI: 10.1021/acs.jpclett.8b01309
J. Phys. Chem. Lett. 2018, 9, 3416−3424

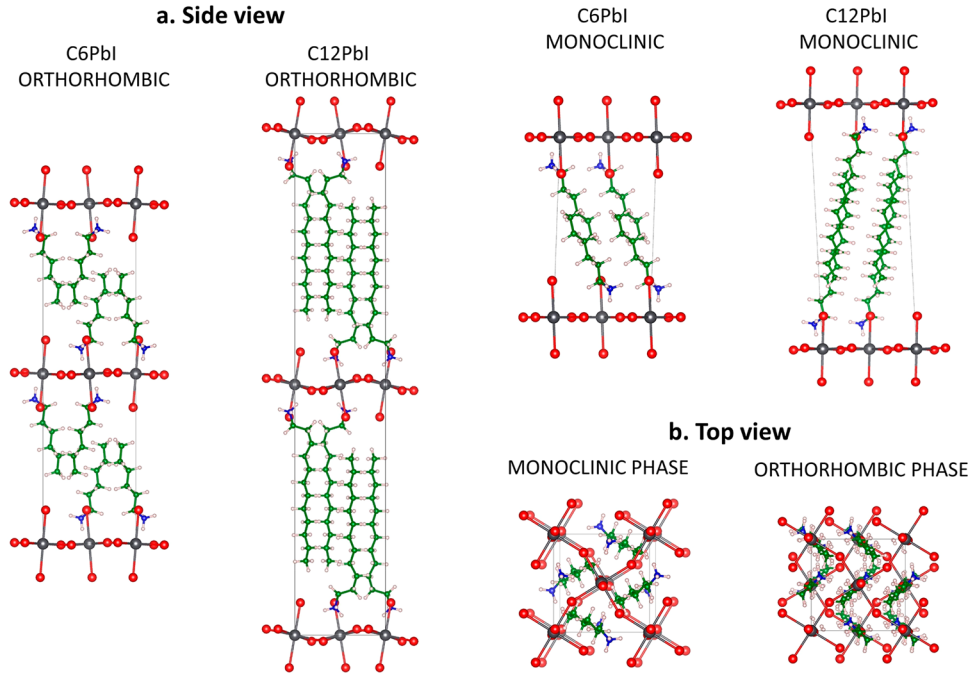

Figure 1. Crystal structure of the investigated monoclinic and orthorhombic phases of C6PbI and C12PbI layered perovskites: (a) side view and (b) top view. Color scale is lead, black; iodine, red; carbon, green; nitrogen, blue; and hydrogen, white.

transition by heating above 315 K.[33] In the present work, we perform density functional theory (DFT)[37,38] and time-dependent DFT (TDDFT)[39] calculations within periodic boundary conditions,[40] considering the monoclinic and orthorhombic polymorphs of C6PbI and C12PbI, whose structures are depicted in Figure 1. We investigate the variation of the electronic properties of these 2D perovskites, considering both the effect of the length of the organic alkyl chain and of the crystalline lattice. Our predictions demonstrate that the chain length indirectly influences the band gap and the effective masses of the electronic properties of layered 2D perovskites via the distortion of the PbI6 octahedra, while not affecting the exciton-binding energy. Thus, the length of the organic component is revealed to be a suitable parameter for tuning the optoelectronic response of 2D layered perovskite materials.

Starting from the crystallographic structures reported by Billings and Lemmerer for the monoclinic ($P2/1a$) and orthorhombic ($Pbca$) phases of C6PbI and C12PbI (Figure 1),[31,33] we first performed structural DFT relaxations of the atomic positions by keeping fixed both the cell parameters and the space group. Ionic forces are evaluated using the PBE exchange–correlation functional,[41] along with the Grimme DFT-D2 method,[42] which is crucial to take into account the van der Waals interactions between organic chains. A detailed description of the computational setup is reported in Methods. Subsequently, we analyzed the electronic properties of these materials, with a special focus on the band gap, band structure, and effective masses.

Before proceeding, we address an important methodological aspect. The quantitative prediction of the band gap of organometal halide perovskites requires considering both relativistic, spin–orbit coupling (SOC) effects and an accurate treatment of electronic exchange and correlation.[43−47] In the case of 3D, $CH_3NH_3PbI_3$ perovskites, it was shown that spin–orbit coupling closes the band gap by 1.0 eV,[44] while a proper account of exchange and correlation (obtained via many-body GW approximation[45,46] or hybrid functionals[47]) opens it by 1.1 eV. As a result, the $CH_3NH_3PbI_3$ band gap estimated at standard GGA (PBE) (1.45−1.65 eV) and neglecting SOC[9,48] is in reasonable agreement with the experimental data (1.5−1.7 eV).[49,50] In contrast, for 2D lead-iodide perovskites, the contribution from exchange–correlation overcomes that from SOC, hence resulting in a band gap opening, when going from standard GGA to more accurate GW+SOC or hybrid DFT +SOC calculations.[23,51] Here, we expand the analysis, looking specifically at the relative contributions to band gap opening induced by shifts in the valence and conduction band edges (VBE and CBE, respectively). It is worth noting that in the case of solid-state calculations, the orbital energies have no absolute meaning,[52] and a consistent inner energy reference is thus needed to compare the results from different calculations, as targeted here. In analogy with Menendez-Proupin,[47] we have thus chosen the average electrostatic potential within the crystalline cell as the energy reference for the position of the VBE and CBE, and we have used the hybrid PBE0 exchange–correlation functional[53] to correct for the self-interaction error in GGA. In Figure 2a, we report the position of the VBE and CBE both with and without SOC and when adopting the PBE versus PBE0 functional, in the case of monoclinic C6PbI where a band gap of ∼2.7 eV has been measured.[36] The band gap predicted for C6PbI at the PBE level and without SOC is 2.04 eV. In turn, including SOC results in a closing of the band gap by 0.66 eV, which is almost completely associated with a downshift by 0.71 eV of the CBE. The selective influence of SOC on the conduction band is due to the fact that this crystalline orbital is mainly composed by 6p orbitals from lead and hence is particularly sensitive to relativistic effects owing to its large mass. The down-shift of CBE has been already explained in the past as being due to SOC-induced splitting of the $j = 1/2$ and $j = 3/2$ total angular momenta components.[43,44] On the contrary, a refined description of the exchange interactions via hybrid PBE0 functional with 30% Hartree–

DOI: 10.1021/acs.jpclett.8b01309
J. Phys. Chem. Lett. 2018, 9, 3416−3424

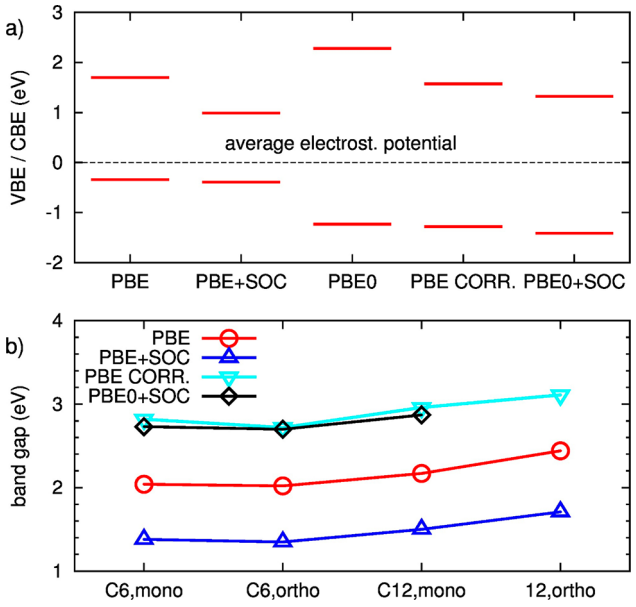

Figure 2. (a) Energy of the valence and conduction band edges (VBE and CBE, respectively) for C6PbI monoclinic perovskite, using PBE, PBE+SOC, PBE0, PBE corrected (CORR, vide infra), and PBE0+SOC. The zero energy corresponds to the averaged electrostatic potential in the cell. (b) Band gap of the four investigated systems computed at the various levels of theory.

Fock (HF) exchange opens the band gap by 1.47 eV, involving both a downshift of 0.89 eV of the VBE and an upshift of 0.58 eV of the CBE. Interestingly, by correcting the results from PBE calculations with the contributions obtained independently from SOC and PBE0 calculations, a final band gap of 2.85 eV in close agreement to the experimental value is obtained (PBE CORR in Figure 2a). Finally, the explicit PBE0+SOC calculation with 30% HF exchange provides a similar band gap of 2.73 eV. In other words, the inclusion of 30% HF exchange in conjunction with SOC is found to reproduce at best the experimental band gap (see the Supporting Information). The changes in the energetics of the VBE and CBE with the computational approach follow the same trend in the other systems (see the Supporting Information). Summarizing, these calculations confirm the previous indications from the literature: for 2D perovskites, the role of SOC and of exchange−correlation effects in the prediction of the electronic band gap are unbalanced, in striking contrast to the case of 3D $CH_3NH_3PbI_3$ perovskite.[23,51]

We now move on to the comparison of the electronic band gap of the two polymorphs of C6PbI and C12PbI, shown in Figure 2b. As the explicit PBE0+SOC calculation for the orthorhombic phase of C12PbI is computationally too demanding, we here adopted the above-mentioned correction scheme as the best guess of the correct band gap. For C6PbI, the monoclinic and orthorhombic phases show the same band gap of 2.73 eV (PBE0+SOC). For C12PbI, the monoclinic and orthorhombic polymorphs show somewhat different band gap of 2.87 and 3.11 eV, respectively. The comparison of the band gap computed for C6PbI and C12PbI clearly indicates that the length of the alkyl chain plays a significant role, in line with experimental investigations. Tanaka et al. in fact observed a blue shift of the ultraviolet−visible (UV−vis) absorption band of alkyl lead iodide layered perovskites with the length of the organic chain.[34] It is worth mentioning that the first optical absorption band in these materials is excitonic in nature,[34−36] but we speculate at this point that the observed blue shift of the excitonic transition with the length of the alkyl chain mimics that of the electronic band gap, which is confirmed by TDDFT calculations below.

Hence, for layered 2D perovskites, longer alkyl chains result in a larger band gap, which in addition depend on crystal structure. The same trend is observed for the effective masses summarized in Table 1. The effective masses within the perovskite plane are similar for the two C6PbI polymorphs and amount to 0.25 and 0.20 (in units of electron mass) for holes and electrons, respectively. C12PbI features larger effective masses, both in the monoclinic and, to a larger degree, orthorhombic phases. Compared to the analogue 3D $CH_3NH_3PbI_3$ perovskite, all the layered perovskites investigated here show larger electron and hole effective masses, even within the perovskite plane, hence suggesting worse transport properties within the inorganic component. In the direction orthogonal to the inorganic plane ($\Gamma \rightarrow \langle 001 \rangle$), layered perovskites are expectedly characterized by infinite effective masses, because of the insulating organic spacer. The effective masses computed for electrons and holes for C6PbI and C12PbI are comparable, as in the 3D case, hence indicating an ambipolar character for the charge transport properties.[45] The atomic density of states plots of these four systems are reported in the Supporting Information.

Two possible mechanisms can be invoked to explain the dependence of the band gap on alkyl chain length and crystalline structure: the first is rooted in electronic confinement effects, and the second stems from structural distortions. The confinement mechanism is at the basis of the larger band

Table 1. Effective Masses for Holes (h) and Electrons (e) and Corresponding Exciton Reduced Mass (μ) for the Monoclinic and Orthorhombic Structures of Layered C6PbI and C12PbI Perovskites[a]

	$CH_3NH_3PbI_3$			C6PbI						C12PbI					
	tetragonal			monoclinic			orthorhombic			monoclinic			orthorhombic		
	h	e	μ	h	e	μ	h	e	μ	h	e	μ	h	e	μ
in-plane															
G→100	0.15	0.13	0.07	0.24	0.19	0.11	0.24	0.18	0.10	0.33	0.25	0.14	0.51	0.32	0.20
G→010	0.15	0.13	0.07	0.25	0.19	0.11	0.25	0.19	0.11	0.35	0.24	0.14	0.49	0.34	0.20
G→110	0.17	0.14	0.08	0.25	0.20	0.11	0.50	0.38	0.22	0.35	0.24	0.14	0.98	0.67	0.40
out-of-plane															
G→001	0.16	0.11	0.07	∞	∞	∞	∞	∞	∞	∞	∞	∞	∞	∞	∞

[a]Effective masses computed for the tetragonal phase of 3D, $CH_3NH_3PbI_3$ perovskite are reported, as reference. Effective masses are obtained from the PBE+SOC level of theory.

DOI: 10.1021/acs.jpclett.8b01309
J. Phys. Chem. Lett. 2018, 9, 3416−3424

gap observed for 2D layered perovskites (2.7 eV for C6)[36] compared to that for the 3D $CH_3NH_3PbI_3$ analogue (1.5−1.7 eV)[49,50] and is related to the spatial separation between inorganic sheets (spatial confinement) and to the difference in the dielectric response of the inorganic and the organic component (dielectric confinement).[36,54,55] Even et al. intensively studied the dielectric confinement mechanism in hybrid lead halide perovskites, investigating the change in energy levels as a function of parameters as the length of the organic component and the number of inorganic layers composing the perovskite (from 5 layers down to 1, as in the present case).[56−58] On the basis of effective models, these authors indicated ∼0.1 eV band gap increase when increasing the barrier length, that is the length of the organic spacer, from 10 to 15 Å,[56] roughly corresponding to the change in interlayer distance when going to C6 to C12 cations. One might therefore argue that, while for the longer C12 alkyl chain the electronic confinement is fully effective, a small residual communication among the inorganic planes still prevails for the shorter C6 chain, which in turn might result in a closing of the band gap for this compound. Alternatively, the indirect role of the organic cation on the electronic properties of hybrid perovskite has been already pointed out in the case of 3D systems, where increased octahedra rotations are associated with increase of the band gap owing to reduced wave function overlap.[48,59] A simple computational experiment aimed to discriminate these two effects consists of taking the structure from the C6PbI compound and substituting the organic C6 cations with the C12, and vice versa for the C12PbI compound (the original and "organic-substituted" structures are compared in the Supporting Information). In this way, assuming the band gap change is dictated by the spatial confinement effect, we should observe a sizable change in the band gap upon substitution of the organic cation. Actually, negligible band gap change is observed upon substituting the C6 organic cations with longer C12 cations in C6PbI perovskite, from 2.02 to 2.07 eV (as determined using PBE without spin−orbit coupling), hence indicating a very small contribution from confinement effects. A slightly larger contribution is observed for C12PbI, whose band gap closes from 2.44 to 2.34 eV upon substituting the C12 with shorter C6 alkyl chains. We hence have dug further on the inorganic structure of the C6PbI and C12PbI polymorphs. Both monoclinic and orthorhombic lattices contain only two PbI_6 octahedra per sheet within the cell and differ by their stacking, eclipsed-like and staggered-like for monoclinic and orthorhombic, respectively (see Figure 1). Because of the use of the space group symmetry, the number of nonequivalent Pb−I bond lengths and Pb−I−Pb angles reduces respectively to only three bonds (b_1, b_2, and b_3) and two angles (θ and δ), showed in Figure 3a. The corresponding values of these parameters for the investigated systems are summarized in the Supporting Information. Consistently with previous works,[56,58] the 2D maps in Figure 3b, obtained by considering a reference model where the organic cations are substituted by Cesium atoms (see the Supporting Information), describe the dependence of the band gap of layered 2D perovskites with respect to angles θ and δ and the Pb−I bond length. These clearly show that the band gap increases with the Pb−I bond length and the octahedra rotation. Nicely, the band gaps found for the C6PbI and C12PbI polymorphs agree well with the predictions from the 2D maps, as shown in Figure 3b. The two polymorphs of C6PbI show almost the same bond lengths and bond angles, consistent with the similar band gap computed for these

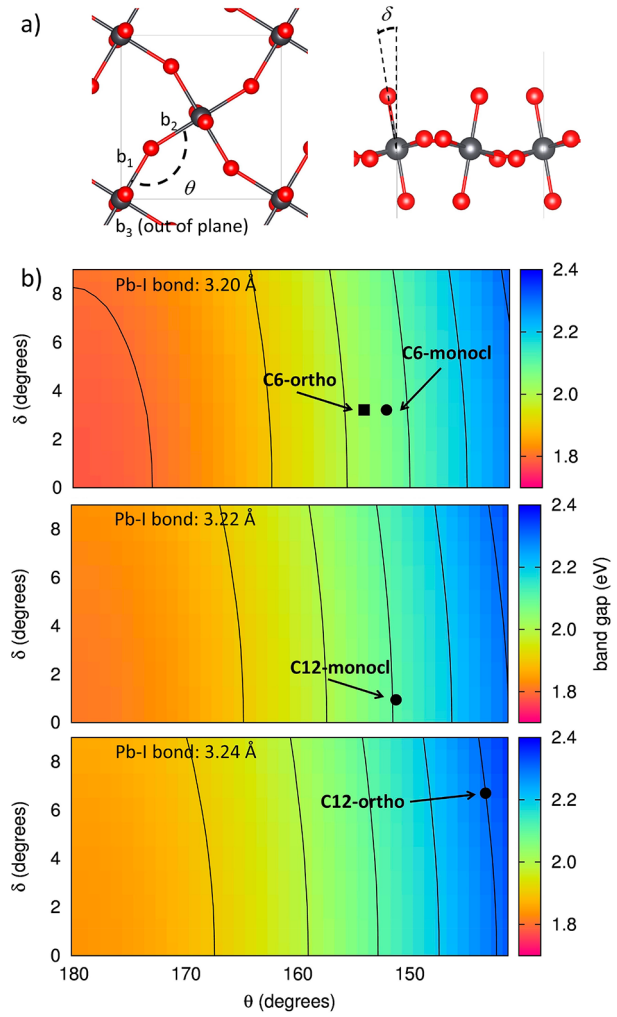

Figure 3. (a) Structural parameters characterizing the inorganic frame: b_1, b_2, and b_3 bond lengths and the θ and δ tilting angles; (b) 2D maps showing the dependence of the band gap (PBE without spin−orbit coupling) on the θ and δ angles, for different average Pb−I bond lengths, obtained for a simplified reference model (see the Supporting Information). The corresponding position in the conformational space for the C6PbI and C12PbI polymorphs is reported.

systems. These systems are characterized by a striking difference between the in plane Pb−I bonds (b_1 and b_2) and the out-of-plane b_3 bond, hence indicating an anisotropic character of the Pb−I bonds within the octahedra. The situation is, instead, different for the two polymorphs of C12PbI. In the monoclinic phase, C12PbI is characterized by similar bond lengths for in-plane and out-of-plane Pb−I bonds. Most importantly, the in-plane Pb−I bonds are systematically 0.01−0.03 Å longer in monoclinic C12PbI, compared to both C6PbI polymorphs. Longer bonds are associated with less effective electronic overlap and are thus in line with the 0.13 and 0.17 eV larger band gap for monoclinic C12PbI, compared to the C6PbI orthorhombic and monoclinic polymorphs, respectively. In the case of orthorhombic C12PbI, in addition to the longer Pb−I bonds, we also find a deviation of angle θ from linearity. Amat et al. already demonstrated the direct connection between this structural parameter and the electronic properties of hybrid perovskites, with less linear θ angle resulting in larger band gap.[11] Hence, the variation of the detailed structure of the inorganic sheet explains not only the

DOI: 10.1021/acs.jpclett.8b01309
J. Phys. Chem. Lett. 2018, 9, 3416−3424

larger band gap of the two C6PbI polymorphs, compared to those of the C12PbI polymorphs, but also the additional dependence of the electronic properties of the C12PbI on the crystal lattice. One could wonder if the constraint on the cell parameters can affect these results. However, also when fully relaxing the unit cell structure, a similar trend in the value of the band gap is predicted and associated with changes in bond lengths b_1, b_2, and b_3 and of angle θ (see the Supporting Information).

What is the rationale for such changes in the inorganic lattice? To address this question, we must now turn our attention to the organic component. In Figure 4, we show the

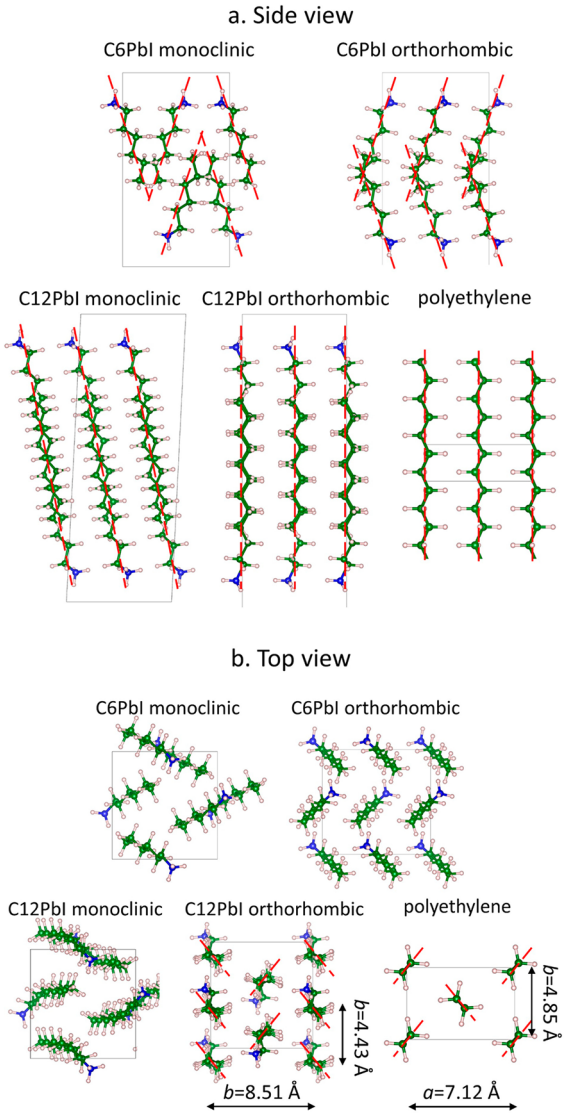

Figure 4. Crystal packing of the four perovskite systems investigated and of polyethylene: (a) side view and (b) top view.

packing of the organic chains of the four investigated systems. The two C6PbI polymorphs show an unusual organization for alkyl chains. The C6 cations in fact do not run parallel but are oriented along two different directions, a packing which is not ideal for maximizing the interactions between CH_2 groups via van der Waals forces. In the monoclinic phase of C12PbI, the cations instead run parallel to each other, allowing for a more effective interaction via van der Waals forces. Finally, for the orthorhombic phase of C12PbI, the alkyl chains present a very peculiar packing, which, at closer inspection, is very reminiscent of that found in the crystal phase of polyethylene.[60,61] The chains in fact run all parallel and interact in an eclipsed configuration (Figure 4a). Moreover, the packing is herringbone and the chain-to-chain distance is very close to the cell parameters of polyethylene (Figure 4b). Thus, the C12PbI orthorhombic phase adopts a structure that seems to promote the most favorable packing of the alkyl chains.

These findings thus bridge the structure of layered perovskites to that of polymeric materials. The crystal structure of 2D organometal halide perovskites can in fact be conveniently considered as the result of two alternating lattices, the organic one and the inorganic one, which compete in driving the overall crystal structure. For short alkyl chains, the weak van der Waals interactions among the CH_2 units are not able to overcome the strong ionic−covalent interactions within the inorganic plane. As a result, the inorganic component imposes its preferred structure at the expense of the organic one, which is forced to adapt an unfavorable packing, as exemplified by the two C6PbI polymorphs. When the length of the organic chain is increased, the van der Waals interactions within the organic component become progressively more and more important, hence competing with the ionic−covalent bonds within the perovskite sheets.[51] Ultimately, for chains long enough, the interactions within the organic component become dominant and impose the overall organization of the layered perovskite, with the consequent modulation of the electronic properties highlighted in Figure 2. Notably, this is the case for the orthorhombic phase of C12PbI, shown in Figure 4, while this is not the case of the monoclinic phase of the same compound, where the inorganic frame shows structure similar to the C6PbI polymorphs, at the expense of a nonideal packing of the organic component. This perspective hence provides the theoretical frame for the interpretation of the orthorhombic → monoclinic transition reported at 315 K for the C12PbI layered perovskite. At low temperature, the balance between the organic−organic and inorganic−inorganic interactions favors the former, hence imposing the organic-dominated, orthorhombic structure in Figure 4. When the temperature is increased, the balance tends to favor the inorganic−inorganic interactions, hence resulting in a phase transition to the inorganic-dominated monoclinic structure. In this sense, our calculations predict sudden changes of the optical properties for C12PbI across the phase transition (T = 315 K), which have been observed previously. Ishihara et al. observed a sudden change in the color of long alkyl chains layered perovskite single crystals, from yellow to orange, when increasing the temperature.[34] The transition is well-documented by temperature-dependent UV−vis absorption and luminescence spectroscopy investigations of decylammonium C10PbI perovskites, showing a steep red shift of ∼0.15 eV for both the absorption and emission band above 270 K, consistent with a phase transition observed around 259 K.[32] The total energies estimated from our fixed cell calculations using the DFT-D2 method predict the correct phase stability for the C6PbI and C12PbI perovskites. For C6PbI, the monoclinic phase is 53 meV (per chemical unit) more stable than the orthorhombic, while for C12PbI the trend is reversed, with the orthorhombic phase being more stable by 104 meV per chemical unit. The larger difference in the stability of the two phases for the C12PbI perovskite is also in line with the higher

DOI: 10.1021/acs.jpclett.8b01309
J. Phys. Chem. Lett. 2018, 9, 3416−3424

temperature at which the phase transition occurs (315 K for the C12, against 268 K for the C6).

Next, we focus on the optical properties of the layered perovskites. In light of the strong excitonic character of these materials,[35,36] the proper description of their optical response requires accounting for electron−hole interaction. Solving the Bethe−Salpeter equation on the basis of a well-converged GW electronic structure hence appears to be the method of choice.[62] On the other hand, such an approach is prohibitively demanding in the present case, due of the large size of the crystals investigated, and we hence adopted the cheaper time-dependent DFT method,[39,63] exploiting the *turbo_tddft* code from the Quantum-Espresso suite.[64] The calculations were performed for the monoclinic phase of C6PbI and C12PbI. Unfortunately, the current implementation of the *turbo_tddft* code does not include spin−orbit coupling, which we showed to be important for the determination of the electronic band gap (see Figure 2). To circumvent this problem, we performed TDDFT calculations using DFT functionals encompassing different amounts of exact exchange, so as to best reproduce the band gap value. Namely, we performed calculations using (i) PBE functional, with full DFT/GGA exchange; (ii) PBE0 functional, with 15% of Hartree−Fock (HF) exchange; and (iii) with 30% of HF exchange, consistent with the previous ground-state calculations in Figure 2.

The optical spectra computed for monoclinic C6PbI and C12PbI at the different levels of theory are reported in Figure 5.

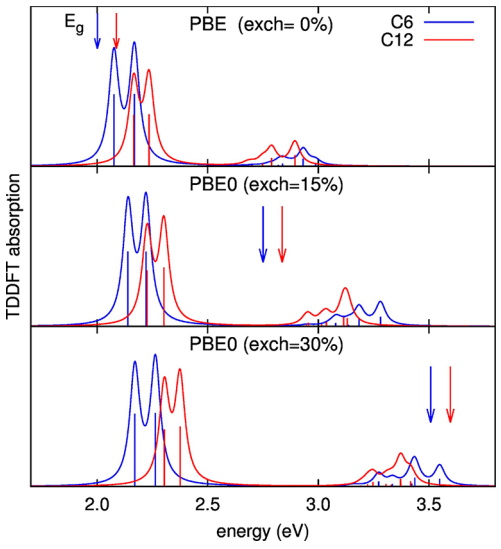

Figure 5. TDDFT-computed absorption spectrum for the monoclinic phase of C6PbI and C12PbI, using PBE exchange−correlation functional and PBE0 15% and 30% exact exchange. Vertical bars correspond to the energy of the excited states. The band gap (E_g) of the two compounds at the different levels of theory are also indicated.

For the sake of completeness, the electronic band gap (E_g) of these materials is also indicated. UV−vis absorption measurements from the literature clearly detect an excitonic transition for C6PbI at 2.37 eV and find the corresponding transition for C12PbI blue-shifted by 0.20 eV.[25] The excitonic feature is followed by broader absorption at higher energies, assigned to direct band-to-band transitions. Reflective optical measurements provide an estimate for the exciton binding energy of 0.36 eV in C6PbI.[36] TDDFT calculations yield two intense features in the low-energy part of the spectrum, at an energy between 2.1 and 2.4 eV, in good agreement with the measured excitonic transition. The calculations also nicely reproduce the blue shift of the excitonic bands, going from C6PbI to C12PbI, which parallels the increase of the electronic band gap discussed previously. We can thus safely conclude that the length of the alkyl chain affects the optical response of layered lead-iodide perovskite by tuning the band gap, while the exciton binding energy remains similar.

Both the energy computed for the two lowest-energy excited states and the blue shift from C6PbI to C12PbI are negligibly affected by the amount of exact exchange. On the other hand, this is not the case for the exciton binding energy, defined as the difference between the electronic band gap and the energy of the lowest excited state. PBE calculations provide negligible (even negative) exciton binding energy. As result, the underestimation of the band gap (as discussed in Figure 2) and of the binding energy cancel out, resulting in a fortuitous agreement against experiment for the excitonic energy. The PBE0 calculation with 15% of exact exchange instead provides a reasonable estimate both for the band gap (2.75 eV from DFT against 2.7[36] for C6) and for the exciton binding energy, ∼0.6 eV. The PBE0 calculation with 30% exact exchange, in turn, overestimates both the band gap and the binding energy, by ∼0.8 eV, hence providing again a fortuitously correct estimate of the energy for the excitonic transition. The exact exchange has thus an important role in dictating not only the band gap, as widely reported in the literature,[45−47] but also the exciton binding energy.

As a last note, we quickly comment on the twin excitonic feature predicted by our TDDFT calculations. Closer inspection shows that this feature is related to the presence of two distinct excited states, lying close in energy for both C6PbI and C12PbI perovskites and mainly consisting of electronic transitions from the HOCO → LUCO and HOCO → LUCO+1 orbitals, respectively (where HOCO and LUCO stand for highest occupied and lowest unoccupied crystalline orbitals, respectively). The shape of these orbitals is reported in the Supporting Information, for the sake of completeness. Notably, these low-lying and second low-lying excited states are polarized within the plane of the inorganic sheet, along the *a* and *b* crystalline axes, respectively. The small (∼0.1 eV) energy difference for these two excited states, shown in Figure 5 for both C6PbI and C12PbI, is fully consistent with the small energy difference (∼0.1 eV) between the LUCO and LUCO+1 energy, as computed at the PBE and PBE0 (15 and 30% of Fock exchange) levels of theory. By contrast, the higher-lying excited states are instead mainly dominated by other electronic transitions involving other crystalline orbitals (see the Supporting Information) which are at least 0.5 eV from the frontier HOCO and LUCO/LUCO+1 orbitals, hence resulting in much larger excitation energy. The presence of this doublet separated by more than 0.5 eV from higher-energy excited states thus simply reflects the density of states of the corresponding ground-state electronic structure. In this sense, the spin−orbit coupling contribution is lacking in these TDDFT calculations and will be considered for future studies, as it lies beyond the scope of the present work, which focuses on the effect of the organic cation in tuning the electronic properties of layered perovskites. UV−vis spectra measured on layered perovskites show typical poor resolution, due to thermal disorder and/or to the morphology of the material. However, at very low temperature, it is possible to resolve a doublet composed of two similar intensity peaks or giving rise

DOI: 10.1021/acs.jpclett.8b01309
J. Phys. Chem. Lett. 2018, 9, 3416−3424

to a single peak with asymmetric line shape, as in refs 25 and 34, hence supporting the presence of two distinct excited states. However, we believe that the assignment of the experimental doublet to the two calculated excited states is premature. The inclusion of spin−orbit coupling in fact is known to split the LUCO and LUCO+1 state[43,44] and is hence expected to separate the doublet components. While more work is needed toward a full rationalization of the optical properties of layered 2D perovskites, our calculations demonstrate that the length of the alkyl chain affects the optical properties of layered perovskite essentially through their effect on the fundamental band gap.

Layered 2D organometal halide ABX4 perovskite are systems with great potential for optoelectronic applications because of their wide chemical flexibility. Chemical design can provide them with unique specific functionalities, such as narrow and color-tunable emission[17−20] and broad-unresolved photoluminescence from long-lived f-centers,[21−25] ideal for lighting applications. These systems showed positive performance also for solar cells with improved stability toward chemical degradation and operate at high open-circuit voltage.[26−28] In this work, we used periodic DFT and TDDFT calculations to investigate the effect of the length of alkyl organic chains in dictating the electronic and optical properties of layered lead-iodide perovskites. We have performed structural relaxations and band structure calculations of alkyl, lead iodide perovskites, considering the hexylammonium (C6) and the dodecylammonium (C12) organic compounds as representative for short and long organic cations, respectively. We have shown that the length of the organic alkyl chain actually affects the electronic properties of the material, with longer chains resulting in larger band gaps, in good agreement with experimental findings,[25,34] and heavier effective masses for both electrons and holes, while no effect is observed on the exciton binding energy, obtained from TDDFT simulations. We have also demonstrated that this effect has a structural origin and is due to an organic-driven distortion of the structure of PbI6 octahedra in the presence of long alkyl chains. The general idea emerging from this work is that the inorganic and the organic component tend to impose their reciprocal favorite crystal packing, possibly competing with each other. For short alkyl chains, the strong ionic−covalent interactions taking place in the inorganic sheets dominate over the weak van der Waals interactions taking place in the organic component. However, when the length of the alkyl chains is increased, the latter interactions become increasingly more important. This fact is epitomized in the C12PbI orthorhombic phase, where the organic component assumes the same packing as that of polyethylene, which represents the thermodynamically most convenient packing for long alkyl chains. In this perspective, also the low-temperature orthorhombic → monoclinic phase transition of C12PbI can be explained as a transition from the low-temperature, organic-dominated structure to the high-temperature, inorganic-dominated structure. The band gap reduction prompted by the phase transitions finds experimental confirmation in a previous study, where a sudden red shift of both the absorption and emission bands has been found for decylammonium C10PbI perovskite, at 270 K,[34] in good correspondence with the 260 K reported phase transition.[33]

By highlighting the role of the organic component, the present work individuates a way to tune the optoelectronic response of layered 2D perovskites resting on the cohesive strength holding the organic component together. Here, we focused on the length of alkyl chains, but many other chemically tunable parameters can be envisaged, for instance by considering organic components interacting via $\pi-\pi$ interactions or considering chains carrying hydrogen bonding units (as in the case of polyamides).

METHODS

Periodic DFT calculations were performed in the planewave/pseudopotential formalism, as implemented in the Quantum Espresso suite program.[40] For the atomic relaxation, we resorted to ultrasoft pseudopotentials, along with a cutoff of 25 and 200 Ry for the expansion of the wave function and of the electronic density, respectively. This setup has been successfully used for the prediction of structural properties of 3D perovskites.[48] For the calculation of the electronic structure, we instead shifted to norm-conserving pseudopotentials, using 50 and 200 Ry cutoff for the wave function and the electronic density, respectively. All calculations were performed using a homogeneous mesh of the first Brillouin zone of $4 \times 4 \times 1$, in the Monkhorst−Pack scheme,[65] where the less dense mesh was used for the direction orthogonal to the inorganic plane. The only exception is for the calculations with hybrid PBE0 functional, where, in light of the high computational cost, we were forced to calculate the band gap only at the Γ point of the first Brillouin zone.

ASSOCIATED CONTENT

Supporting Information

The Supporting Information is available free of charge on the ACS Publications website at DOI: 10.1021/acs.jpclett.8b01309.

Fitting of the Hartree−Fock percentage in PBE0+SOC calculations to reproduce the experimental band gap of C6PbI; valence and conduction band edges, referred to the averaged electrostatic potential in the cell, computed for the C6PbI and C12PbI polymorphs at various levels of theory; atomic density of states (DOS) for the four investigated systems, calculated at the PBE+SOC level of theory; C6PbI and C12PbI models with substituted C6 and C12 organic spacers; detailed bond lengths and angles for the inorganic frame of the systems investigated; model structure used for the calculation of the 2D maps in Figure 3b; internal Pb−I bond lengths and θ angle for relaxed cells; details of the 15 lowest-energy excited states (energy, dipole, main single-particle excitations contributing to the excited states) for monoclinic phase of C6PbI and C12PbI; shape of the HOCO, LUCO, and LUCO+1 crystalline orbitals (PDF)

AUTHOR INFORMATION

Corresponding Author

*E-mail: claudio.quarti@umons.ac.be.

ORCID

Claudio Quarti: 0000-0002-5488-1216

Notes

The authors declare no competing financial interest.

ACKNOWLEDGMENTS

The work was supported by the Interuniversity Attraction Pole program of the Belgian Federal Science Policy Office (PAI 6/27) and FNRS-F.R.S. Computational resources have been provided by the Consortium des Équipements de Calcul

DOI: 10.1021/acs.jpclett.8b01309
J. Phys. Chem. Lett. 2018, 9, 3416−3424

Intensif (CÉCI), funded by the Fonds de la Recherche Scientifique de Belgique (F.R.S.-FNRS) under Grant No. 2.5020.11. D.B. is a FNRS Research Director. The authors thank E. Radicchi, D. Meggiolaro, E. Mosconi, and F. De Angelis for useful discussions.

REFERENCES

(1) Kojima, A.; Teshima, K.; Shirai, Y.; Miyasaka, T. Organometal Halide Perovskites as Visible-Light Sensitizers for Photovoltaic Cells. *J. Am. Chem. Soc.* **2009**, *131*, 6050−6051.
(2) Im, J.-H.; Lee, C.-R.; Lee, J.-W.; Park, S.-W.; Park, N.-G. 6.5% Efficient Perovskite Quantum-Dot-Sensitized Solar Cell. *Nanoscale* **2011**, *3*, 4088−4093.
(3) Burschka, J.; Pellet, N.; Moon, S.-J.; Humphry-Baker, R.; Gao, P.; Nazeeruddin, M. K.; Graetzel, M. Sequential Deposition as a Route to High-Performance Perovskite-Sensitized Solar Cells. *Nature* **2013**, *499*, 316−319.
(4) Liu, M.; Johnston, M. B.; Snaith, H. J. Efficient Planar Heterojunction Perovskite Solar Cells by Vapour Deposition. *Nature* **2013**, *501*, 395−398.
(5) Zhou, H.; Chen, Q.; Li, G.; Luo, S.; Song, T.-B.; Duan, H.-S.; Hong, Z.; You, J.; Liu, Y.; Yang, Y. Interface Engineering of Highly Efficient Perovskite Solar Cells. *Science* **2014**, *345*, 542−546.
(6) Jeon, N. J.; Noh, J. H.; Yang, W. S.; Kim, Y. C.; Ryu, S.; Seo, J.; Seok, S. I. Compositional Engineering of Perovskite Materials for High-Performance Solar Cells. *Nature* **2015**, *517*, 476−480.
(7) Yang, W. S.; Park, B.-W.; Jung, E. H.; Jeon, N. J.; Kim, Y. C.; Lee, D. U.; Shin, S. S.; Seo, J.; Kim, E. K.; Noh, J. H.; et al. Iodide Management in Formamidinium-Lead-Halide−Based Perovskite Layers for Efficient Solar Cells. *Science* **2017**, *356*, 1376−1379.
(8) Green, M.; Bein, T. Photovoltaics: Perovskite Cells Charge Forward. *Nat. Mater.* **2015**, *14*, 559−561.
(9) Umebayashi, T.; Asai, K.; Kondo, T.; Nakao, A. Electronic Structures of Lead Iodide Based Low-Dimensional Crystals. *Phys. Rev. B: Condens. Matter Mater. Phys.* **2003**, *67*, 155405.
(10) Mosconi, E.; Amat, A.; Nazeeruddin, M. K.; Graetzel, M.; De Angelis, F. First-Principles Modeling of Mixed Halide Organometal Perovskites for Photovoltaic Applications. *J. Phys. Chem. C* **2013**, *117*, 13902−13913.
(11) Amat, A.; Mosconi, E.; Ronca, E.; Quarti, C.; Umari, P.; Nazeeruddin, M. K.; Graetzel, M.; De Angelis, F. Cation-Induced Band Gap Tuning in Organohalide Perovskites: Interplay of Spin-Orbit Coupling and Octahedral Tilting. *Nano Lett.* **2014**, *14*, 3608−3616.
(12) Eperon, G. E.; Stranks, S. D.; Menelaou, C.; Johnston, M. B.; Herz, L. M.; Snaith, H. J. Formamidinium Lead Trihalide: A Broadly Tunable Perovskite for Efficient Planar Heterojunction Solar Cells. *Energy Environ. Sci.* **2014**, *7*, 982−988.
(13) Saliba, M.; Matsui, T.; Seo, J.-Y.; Domanski, K.; Correa-Baena, J.-P.; Nazeeruddin, M. K.; Zakeeruddin, S. M.; Tress, W.; Abate, A.; Hagfeldtd, A.; et al. Cesium-Containing Triple Cation Perovskite Solar Cells: Improved Stability, Reproducibility and High Efficiency. *Energy Environ. Sci.* **2016**, *9*, 1989−1997.
(14) Saliba, M.; Matsui, T.; Domanski, K.; Seo, J.-Y.; Ummadisingu, A.; Zakeeruddin, S. M.; Correa-Baena, J.-P.; Tress, W. R.; Abate, A.; Hagfeldt, A.; et al. Incorporation of Rubidium Cations into Perovskite Solar Cells Improves Photovoltaic Performance. *Science* **2016**, *354*, 206−209.
(15) Mitzi, D. Templating and Structural Engineering in Organic-Inorganic Perovskites. *J. Chem. Soc., Dalton Trans.* **2001**, *1*, 1−12.
(16) Mitzi, D. Solution-Processed Inorganic Semiconductors. *J. Mater. Chem.* **2004**, *14*, 2355−2365.
(17) Pradeesh, K.; Baumberg, J. J.; Prakash, G. V. In Situ Intercalation Strategies for Device-Quality Hybrid Inorganic-Organic Self-Assembled Quantum Wells. *Appl. Phys. Lett.* **2009**, *95*, 033309.
(18) Yuan, M.; Quan, L. N.; Comin, R.; Walters, G.; Sabatini, R.; Voznyy, O.; Hoogland, S.; Zhao, Y.; Beauregard, E. M.; Kanjanaboos, P.; et al. Perovskite Energy Funnels for Efficient Light-Emitting Diodes. *Nat. Nanotechnol.* **2016**, *11*, 872−877.
(19) Dou, L.; Wong, A. B.; Yu, Y.; Lai, M.; Kornienko, N.; Eaton, S. W.; Fu, A.; Bischak, C. G.; Ma, J.; Ding, T.; et al. Atomically Thin Two-Dimensional Organic-Inorganic Hybrid Perovskites. *Science* **2015**, *349*, 1518−1521.
(20) Kumar, S.; Jagielski, J.; Yakunin, S.; Rice, P.; Chiu, Y.-C.; Wang, M.; Nedelcu, G.; Kim, Y.; Lin, S.; Santos, E. J. G.; et al. Efficient Blue Electroluminescence Using Quantum-Confined Two-Dimensional Perovskites. *ACS Nano* **2016**, *10*, 9720−9729.
(21) Dohner, E. R.; Hoke, E. T.; Karunadasa, H. I. Self-Assembly of Broadband White-Light Emitters. *J. Am. Chem. Soc.* **2014**, *136*, 1718−1721.
(22) Hu, T.; Smith, M. D.; Dohner, E. R.; Sher, M.-J.; Wu, X.; Trinh, T. M.; Fisher, A.; Corbett, J.; Zhu, X.-Y.; Karunadasa, H. I.; et al. Mechanism for Broadband White-Light Emission from Two-Dimensional (110) Hybrid Perovskites. *J. Phys. Chem. Lett.* **2016**, *7*, 2258−2263.
(23) Cortecchia, D.; Neutzner, S.; Kandada, A. R. S.; Mosconi, E.; Meggiolaro, D.; De Angelis, F.; Soci, C.; Petrozza, A. Broadband Emission in Two-Dimensional Hybrid Perovskites: The Role of Structural Deformation. *J. Am. Chem. Soc.* **2017**, *139*, 39−42.
(24) Mao, L.; Wu, Y.; Stoumpos, C. C.; Wasielewski, M. R.; Kanatzidis, M. G. White-Light Emission and Structural Distortion in New Corrugated Two-Dimensional Lead Bromide Perovskites. *J. Am. Chem. Soc.* **2017**, *139*, 5210−5215.
(25) Booker, E. P.; Thomas, T. H.; Quarti, C.; Stanton, M. R.; Dashwood, C. D.; Gillett, A. J.; Richter, J. M.; Pearson, A. J.; Davis, N. J. L. K.; Sirringhaus, H.; et al. Formation of Long-Lived Color Centers for Broadband Visible Light Emission in Low-Dimensional Layered Perovskites. *J. Am. Chem. Soc.* **2017**, *139*, 18632−18639.
(26) Cao, D. H.; Stoumpos, C. C.; Farha, O. K.; Hupp, J. T.; Kanatzidis, M. G. 2d Homologous Perovskites as Light-Absorbing Materials for Solar Cell Applications. *J. Am. Chem. Soc.* **2015**, *137*, 7843−7850.
(27) Tsai, H.; Nie, W.; Blancon, J.-C.; Stoumpos, C. C.; Asadpour, R.; Harutyunyan, B.; Neukirch, A. J.; Verduzco, R.; Crochet, J. J.; Tretiak, S.; et al. High-Efficiency Two-Dimensional Ruddlesden−Popper Perovskite Solar Cells. *Nature* **2016**, *536*, 312−316.
(28) Grancini, G.; Roldán-Carmona, C.; Zimmermann, I.; Mosconi, E.; Lee, X.; Martineau, D.; Narbey, S.; Oswald, F.; De Angelis, F.; Graetzel, M.; et al. One-Year Stable Perovskite Solar Cells by 2d/3d Interface Engineering. *Nat. Commun.* **2017**, *8*, 15684.
(29) Milot, R. L.; Sutton, R. J.; Eperon, G. E.; Haghighirad, A. A.; Hardigree, J. M.; Miranda, L.; Snaith, H. J.; Johnston, M. B.; Herz, L. M. Charge-Carrier Dynamics in 2d Hybrid Metal-Halide Perovskites. *Nano Lett.* **2016**, *16*, 7001−7007.
(30) Gan, L.; Li, J.; Fang, Z.; He, H.; Ye, Z. Effects of Organic Cation Length on Exciton Recombination in Two-Dimensional Layered Lead Iodide Hybrid Perovskite Crystals. *J. Phys. Chem. Lett.* **2017**, *8*, 5177−5183.
(31) Billing, D. G.; Lemmerer, A. Synthesis, Characterization and Phase Transitions in the Inorganic-Organic Layered Perovskite-Type Hybrids $[(C_nh_{2n+1}nh_3)_2pbi_4)]$, N = 4, 5 and 6. *Acta Crystallogr., Sect. B: Struct. Sci.* **2007**, *63*, 735−747.
(32) Lemmerer, A.; Billing, D. G. Synthesis, Characterization and Phase Transitions in the Inorganic-Organic Layered Perovskite-Type Hybrids $[(C_nh_{2n+1}nh_3)_2pbi_4)]$, N = 7, 8, 9 and 10. *Dalton Trans.* **2012**, *41*, 1146−1157.
(33) Billing, D. G.; Lemmerer, A. Synthesis, Characterization and Phase Transitions of the Inorganic−Organic Layered Perovskite-Type Hybrids $[(C_nh_{2n+1}nh_3)_2pbi_4]$ (N = 12, 14, 16 and 18). *New J. Chem.* **2008**, *32*, 1736−1746.
(34) Ishihara, T.; Takahashi, J.; Goto, T. Optical Properties Due to Electronic Transitions in Two-Dimensional Semiconductors $(C_nh_{2n+1}nh_3)_2pbi_4$. *Phys. Rev. B: Condens. Matter Mater. Phys.* **1990**, *42*, 11099−11107.
(35) Tanaka, K.; Sano, F.; Takahashi, T.; Kondo, T.; Ito, R.; Ema, K. Two-Dimensional Wannier Excitons in a Layered-Perovskite-Type Crystal $(C_6h_{13}nh_3)_2pbi_4$. *Solid State Commun.* **2002**, *122*, 249−252.

DOI: 10.1021/acs.jpclett.8b01309
J. Phys. Chem. Lett. 2018, 9, 3416−3424

(36) Tanaka, K.; Takahashi, T.; Kondo, T.; Umebayashi, T.; Asai, K.; Ema, K. Image Charge Effect on Two-Dimensional Excitons in an Inorganic-Organic Quantum-Well Crystal. *Phys. Rev. B: Condens. Matter Mater. Phys.* **2005**, *71*, 045312.
(37) Hohenberg, P.; Kohn, W. Inhomogeneous Electron Gas. *Phys. Rev.* **1964**, *136*, B864−871.
(38) Kohn, W.; Sham, L. J. Self-Consistent Equations Including Exchange and Correlation Effects. *Phys. Rev.* **1965**, *140*, A1133−A1138.
(39) Runge, E.; Gross, E. K. U. Density-Functional Theory for Time-Dependent Systems. *Phys. Rev. Lett.* **1984**, *52*, 997−1000.
(40) Giannozzi, P.; Baroni, S.; Bonini, N.; Calandra, M.; Car, R.; Cavazzoni, C.; Ceresoli, D.; Chiarotti, G. L.; Cococcioni, M.; Dabo, I.; et al. Quantum Espresso: A Modular and Open-Source Software Project for Quantum Simulations of Materials. *J. Phys.: Condens. Matter* **2009**, *21*, 395502.
(41) Perdew, J. P.; Burke, K.; Ernzerhof, M. Generalized Gradient Approximation Made Simple. *Phys. Rev. Lett.* **1996**, *77*, 3865−3868.
(42) Grimme, S. Semiempirical Gga-Type Density Functional Constructed with a Long-Range Dispersion Correction. *J. Comput. Chem.* **2006**, *27*, 1787−1799.
(43) Even, J.; Pedesseau, L.; Dupertuis, M.-A.; Jancu, J.-M.; Katan, C. Electronic Model for Self-Assembled Hybrid Organic/Perovskite Semiconductors: Reverse Band Edge Electronic States Ordering and Spin-Orbit Coupling. *Phys. Rev. B: Condens. Matter Mater. Phys.* **2012**, *86*, 205301.
(44) Even, J.; Pedesseau, L.; Jancu, J.-M.; Katan, C. Importance of Spin−Orbit Coupling in Hybrid Organic/Inorganic Perovskites for Photovoltaic Applications. *J. Phys. Chem. Lett.* **2013**, *4*, 2999−3005.
(45) Umari, P.; Mosconi, E.; De Angelis, F. Relativistic GW Calculations on $CH_3NH_3PbI_3$ and $CH_3NH_3SnI_3$ Perovskites for Solar Cell Applications. *Sci. Rep.* **2015**, *4*, 4467.
(46) Brivio, F.; Butler, K. T.; Walsh, A.; van Schilfgaarde, M. Relativistic Quasiparticle Self-Consistent Electronic Structure of Hybrid Halide Perovskite Photovoltaic Absorbers. *Phys. Rev. B: Condens. Matter Mater. Phys.* **2014**, *89*, 155204.
(47) Menéndez-Proupin, E.; Palacios, P.; Wahnon, P.; Conesa, J. C. Self-Consistent Relativistic Band Structure of the $Ch_3nh_3pbi_3$ Perovskite. *Phys. Rev. B: Condens. Matter Mater. Phys.* **2014**, *90*, 045207.
(48) Quarti, C.; Mosconi, E.; De Angelis, F. Interplay of Orientational Order and Electronic Structure in Methylammonium Lead Iodide: Implications for Solar Cells Operation. *Chem. Mater.* **2014**, *26*, 6557−6569.
(49) D'Innocenzo, V.; Grancini, G.; Alcocer, M. J. P.; Kandada, A. R. S.; Stranks, S. D.; Lee, M. M.; Lanzani, G.; Snaith, H. J.; Petrozza, A. Excitons Versus Free Charges in Organo-Lead Tri-Halide Perovskites. *Nat. Commun.* **2014**, *5*, 3586.
(50) Schulz, P.; Edri, E.; Kirmayer, S.; Hodes, G.; Cahen, D.; Kahn, A. Interface Energetics in Organo-Metal Halide Perovsite-Based Photovoltaic Cells. *Energy Environ. Sci.* **2014**, *7*, 1377−1381.
(51) Fraccarollo, A.; Cantatore, V.; Boschetto, G.; Marchese, L.; Cossi, M. Ab Initio Modeling of 2d Layered Organohalide Lead Perovskites. *J. Chem. Phys.* **2016**, *144*, 164701.
(52) Kleinman, L. Comment on the Average Potential of a Wigner Solid. *Phys. Rev. B: Condens. Matter Mater. Phys.* **1981**, *24*, 7412−7414.
(53) Adamo, C.; Barone, V. Toward Reliable Density Functional Methods without Adjustable Parameters: The Pbe0Model. *J. Chem. Phys.* **1999**, *110*, 6158−6170.
(54) Keldysh, L. V. Coulomb Interaction in Thin Semiconductor and Semimetal Films. *JETP Lett.* **1979**, *29*, 658−660.
(55) Muljarov, E. A.; Tikhodeev, S. G.; Gippius, N. A. Excitons in Self-Organized Semiconductor/Insulator Superlattices: Pbi-Based Perovskite Compounds. *Phys. Rev. B: Condens. Matter Mater. Phys.* **1995**, *51*, 14370−14378.
(56) Even, J.; Pedesseau, L.; Katan, C. Understanding Quantum Confinement of Charge Carriers in Layered 2d Hybrid Perovskites. *ChemPhysChem* **2014**, *15*, 3733−3741.
(57) Sapori, D.; Kepenekian, M.; Pedesseau, L.; Katan, C.; Even, J. Quantum Confinement and Dielectric Profiles of Colloidal Nanoplatelets of Halide Inorganic and Hybrid Organic-Inorganic Perovskites. *Nanoscale* **2016**, *8*, 6369−6378.
(58) Traore, B.; Pedesseau, L.; Assam, L.; Che, X.; Blancon, J.-C.; Tsai, H.; Nie, W.; Stoumpos, C. C.; Kanatzidis, M. G.; Tretiak, S.; et al. Composite Nature of Layered Hybrid Perovskites: Assessment on Quantum and Dielectric Confinements and Band Alignment. *ACS Nano* **2018**, *12*, 3321−3332.
(59) Motta, C.; El-Mellouhi, F.; Kais, S.; Tabet, N.; Alharbi, F.; Sanvito, S. Revealing Hte Role of Organic Cations in Hybrid Halide Perovskite $Ch_3nh_3pbi_3$. *Nat. Commun.* **2015**, *6*, 7026.
(60) Bunn, C. W. The Crystal Structure of Long-Chain Normal Paraffin Hydrocarbons. The "Shape" of the Ch_2 Group. *Trans. Faraday Soc.* **1939**, *35*, 482−491.
(61) Avitabile, G.; Napolitano, R.; Pirozzi, B.; Rouse, K. R.; Thomas, M. W.; Willis, B. T. M. Low Temperature Crystal Structure of Polyethylene: Results from a Neutron Diffraction Study and from Potential Energy Calculations. *J. Polym. Sci., Polym. Lett. Ed.* **1975**, *13*, 351−355.
(62) Umari, P.; Mosconi, E.; De Angelis, F. Infrared Dielectric Screening Determines the Low Exciton Binding Energy of Metal-Halide Perovskites. *J. Phys. Chem. Lett.* **2018**, *9*, 620−627.
(63) Marques, M. A. L.; Maitra, N. T.; Nogueira, F. M. S.; Gross, E. K. U.; Rubio, A. *Fundamentals of Time-Dependent Density Functional Theory*; Springer-Verlag: Berlin, 2012.
(64) Ge, X.; Binnie, S.; Rocca, D.; Gebauer, R.; Baroni, S. Turbotddft 2.0—Hybrid Functionals and New Algorithms within Time-Dependent Density-Functional Perturbation Theory. *Comput. Phys. Commun.* **2014**, *185*, 2080−2089.
(65) Monkhorst, H. J.; Pack, J. D. Special Points for Brillouin-Zone Integrations. *Phys. Rev. B* **1976**, *13*, 5188−5192.

DOI: 10.1021/acs.jpclett.8b01309
J. Phys. Chem. Lett. 2018, 9, 3416−3424